

A local field emission study of partially aligned carbon-nanotubes by AFM probe

A. Di Bartolomeo,* A. Scarfato, F. Giubileo, F. Bobba, M. Biasucci, and A.M. Cucolo
*Dipartimento di Fisica "E.R. Caianiello", Università degli Studi di Salerno,
 and CNR-INFM Laboratorio Regionale SUPERMAT,
 and INFN Gruppo collegato di Salerno, via S. Allende 84081 Baronissi (SA), Italia*

S. Santucci and M. Passacantando

Dipartimento di Fisica, Università dell'Aquila and INFN, via Vetoio 67010 Coppito (AQ), Italia

(Dated: June 24, 2021)

We report on the application of Atomic Force Microscopy (AFM) for studying the Field Emission (FE) properties of a dense array of long and vertically quasi-aligned multi-walled carbon nanotubes grown by catalytic Chemical Vapor Deposition on a silicon substrate. The use of nanometric probes enables local field emission measurements allowing investigation of effects non detectable with a conventional parallel plate setup, where the emission current is averaged on a large sample area. The micrometric inter-electrode distance let achieve high electric fields with a modest voltage source. Those features allowed us to characterize field emission for macroscopic electric fields up to $250 \text{ V}/\mu\text{m}$ and attain current densities larger than $10^5 \text{ A}/\text{cm}^2$. FE behaviour is analyzed in the framework of the Fowler-Nordheim theory. A field enhancement factor $\gamma \approx 40$ -50 and a turn-on field $E_{\text{turn-on}} \sim 15 \text{ V}/\mu\text{m}$ at an inter-electrode distance of $1 \mu\text{m}$ are estimated. Current saturation observed at high voltages in the I-V characteristics is explained in terms of a series resistance of the order of $\text{M}\Omega$. Additional effects as electrical conditioning, CNT degradation, response to laser irradiation and time stability are investigated and discussed.

PACS numbers: 68.37.-d; 73.63.Fg; 81.07.De

I. INTRODUCTION

Controlled propagation of electrons in vacuum is at the basis of several technological applications, like CRT displays, vacuum electronics, electron microscopy, X-ray generation, electron beam lithography, etc. The most common technique to extract electron from matter is thermionic emission, which requires a source heated at high temperature ($\sim 1000^\circ\text{C}$) and has several drawbacks. Field emission (FE), which involves extraction of electrons from a conducting solid (metal or highly doped semiconductor) by an external electric field, is becoming one of the best alternatives. Indeed, by this method, an extremely high current density with low energy spread of the emitted electrons and with negligible power consumption can be achieved [1, 2, 3].

High macroscopic electric fields of several $\text{kV}/\mu\text{m}$ are required for electrons to tunnel through the surface-to-vacuum potential barrier. Such high fields can be practically obtained by exploiting the local electric field enhancement at the apex of a tip with small radius of curvature. With pointed cathodes, the macroscopic electric field needed for electron emission can be reduced to few $\text{V}/\mu\text{m}$.

For their high aspect ratio (diameter in the nanometer scale and length of several microns), extremely small radius of curvature, unique electric properties, high chemical stability and mechanical strength, carbon nanotubes

(CNTs) [4, 5, 6, 7, 8] can be extraordinary field emitters and interest in their applicability for FE devices has been steadily growing since their discovery in 1991 [9].

Field emission has been observed both from single-walled (SWCNT) and multi-walled (MWCNT) carbon nanotubes, individual or in an ensemble (CNT films). Current densities over 1 Acm^{-2} at macroscopic applied fields of few $\text{V}/\mu\text{m}$ have been reported [10, 11, 12, 13].

In technological applications, films of vertically aligned nanotubes grown or deposited on a substrate have the largest potential: the fabrication is relatively easy and suitable for industrial production, the patterning is possible through optical or electron beam lithography, and, depending on the inter-tube spacing [14], extremely high emission capability can be attained [15, 16, 17, 18, 19].

Over the past ten years, a variety of vertical CNT films, differing for tube type (MW or SW), shape, dimension, density, substrate, etc. have been extensively studied and used in prototype FE devices, like displays, lamps, X-ray tubes, microwave power amplifiers, etc. [20, 21, 22, 23, 24]. However, the unavoidable inhomogeneous composition and morphology of CNT films, even on micrometric areas, make the comprehension of the influence of fabrication and structural parameters on the FE properties a scientific challenge.

Experiments with phosphor screens have evidenced that emission from a CNT film originates from isolated spots. FE current measurements performed by conventional large area anode setups are affected by the dominant contribution of a small subset of highly emitting CNTs that can hide important characteristics of the remaining majority [25, 26]. Therefore, small (possibly nanometric) area anodes are essential for an accurate

*Electronic address: dibant@sa.infn.it

investigation of individual emission site current-voltage (I-V) or current-time (I-t) characteristics and for obtaining statistical data on the spatially or time dependent FE behaviour of thin film emitters.

In this report we present a detailed study of FE performed on a film of partially aligned MWCNTs with an anode consisting of a nanometric AFM/STM probe in a high vacuum chamber. A large amount of experimental data, on different sites of a single sample, allowed a significant statistic analysis of several effects. In the majority of the measurements, we observed a reproducible FE current saturation at high fields, which is explained in terms of a series resistance modified Fowler-Nordheim model. Emission stability and response to radiation, relevant topics for technological applications, are discussed.

II. CNT PRODUCTION

A dense array of vertical and partially aligned carbon nanotubes was produced by catalytic Chemical Vapor Deposition (CVD). A Nickel film of 3 nm was deposited on a silicon substrate (001, p-type, $\rho = 1 - 40\Omega\text{cm}$), covered by a thin layer of SiO_2 (thickness ~ 3 nm), acting as diffusion layer and preventing the formation of NiSi_x (which does not have a catalytic function). Growth of carbon nanotubes was achieved by chemical decomposition of acetylene on clusterized Ni (catalyst) upon heating at about 700°C in NH_3 ambient. Acetylene was injected in the chamber together with ammonia in the ratio $\text{C}_2\text{H}_2/\text{NH}_3$ 1:5. The gas ratio, the chamber temperature and the growth time were the main control parameters.

The average height of the CNTs produced with this procedure was around $15\text{ }\mu\text{m}$ as can be seen from the SEM images shown in Fig. 1. Vertical alignment is due to a crowding effect, i.e. neighbouring tubes supporting each other by van der Waals forces. A TEM analysis (not shown here) revealed that the nanotubes are multi-walled with inner and outer diameters of 5-10 nm and 15-25 nm, respectively.

SEM top view (Fig. 1c) shows also that our film lose verticality in the upper part towards the air surface. This is a non-critical limitation for field emission applications since the nanotubes are stretched and aligned along the cathode-anode direction at typically a quarter of the voltage necessary to trigger emission, regardless of their initial disposition [27, 28].

Particles, that backscattered SEM analysis proved to have a high Ni content, are visible at the upper end of the nanotubes, indicating a weak catalyst adherence to the surface and a dominating "tip growth" mechanism [29].

III. MEASUREMENT SETUP

Field Emission measurements were performed by means of an Omicron UHV STM/AFM system, oper-

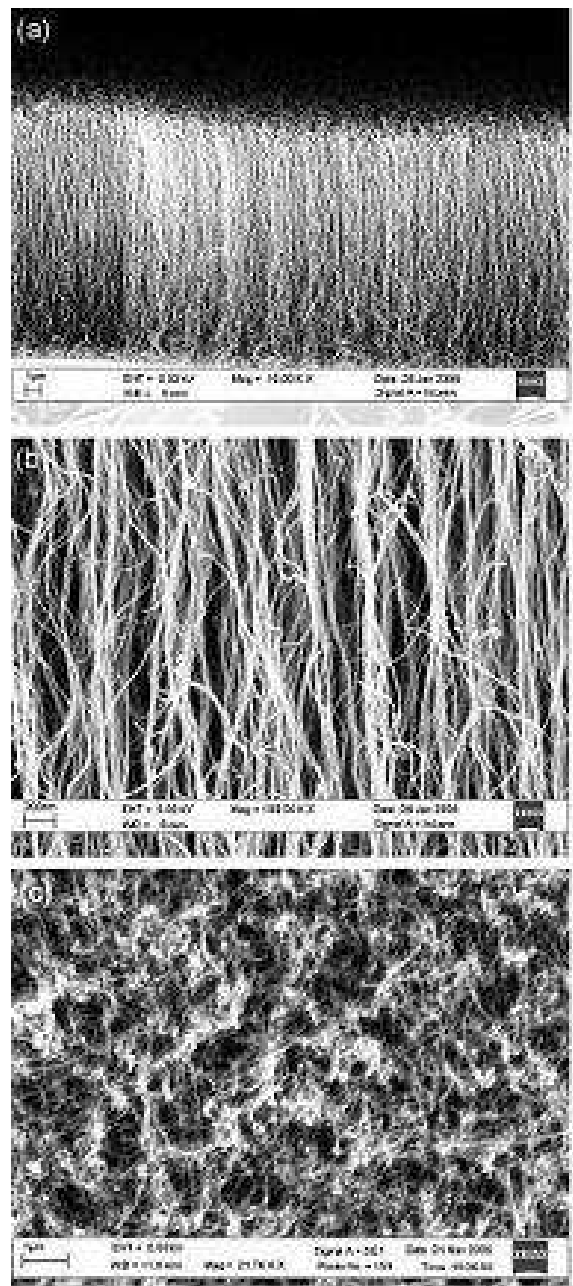


FIG. 1: SEM images of vertically aligned MWCNTs, grown by catalytic chemical vapour deposition on a silicon substrate (area $5\times 5\text{ mm}^2$) with Ni catalyst. (a), (b) lateral views, (c) top view.

ating at room temperature, and connected to a Semiconductor Parameter Analyser Keithley 4200-SCS, working as SMU (source-measurement unit). A detailed scheme for FE apparatus is shown in Fig. 2.

Current measurements were carried out initially in a static vacuum of $10^{-3} - 10^{-4}$ mbar produced by a turbomolecular pump, and successively, to improve the signal to noise ratio, at $10^{-7} - 10^{-8}$ mbar by an ionic pump installation. High vacuum is crucial to reduce the effects of

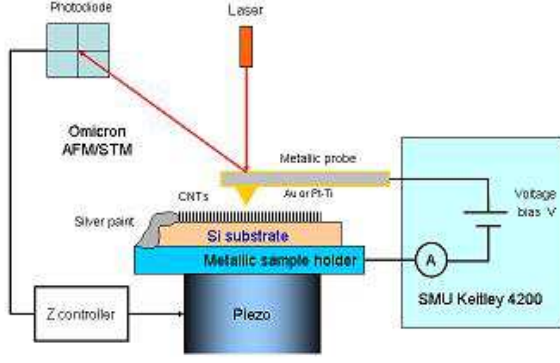


FIG. 2: AFM probe used as counter-electrode for the measurement of the FE current from a vertically aligned array of MWCNTs. The whole apparatus consists of a vacuum chamber hosting an AFM/STM connected to an external source measurement unit.

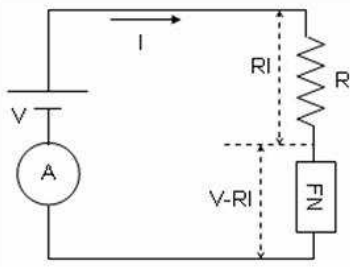


FIG. 3: Schematic representation of the measurement circuit. A is the ammeter, V the voltage source, R the series resistance and FN is the Fowler-Nordheim current device, constituted by the CNT film emitter array and the AFM tip.

adsorbates as O_2 , H_2 , H_2O , N_2 on FE current value and stability (it was shown for example that H_2O increases the emission while O_2 decreases it dramatically [30]; any gas enhances fluctuations).

A two probe method was chosen for its simplicity. The electrical connection of the CNT film and the Si substrate

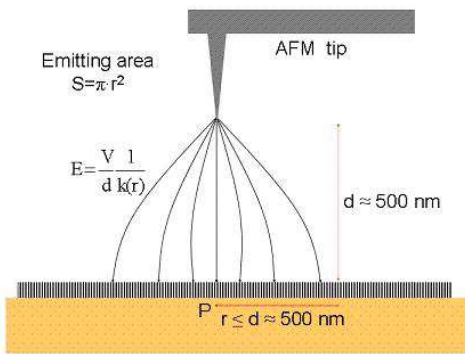


FIG. 4: : Electric field in the region between an AFM tip and a flat CNT emitting surface.

with the metallic sample holder was assured through a spot of silver paint. The equivalent circuit is modelled in Fig. 3, where R is a series resistance accounting for CNTs, interfaces, contacts and wires resistances. Voltage sweeps were performed on the allowed range of -210 to +210 V. The current flowing through the tip was measured with an accuracy better than 1 pA.

Horizontal movements of the tip, with steps of ~ 0.1 nm, covered an area of $5 \times 5 \mu m^2$ and accurate vertical control was over a distance of $2 \mu m$, with resolution better than 0.1 \AA . The AFM tips (Au- or Pt/Ti-coated polysilicon), of conical shape, had aperture of $\sim 30^\circ$, curvature radius ≤ 35 nm, height 20-25 μm . The elastic constant of the cantilever was ~ 40 N/m and the resonant frequency ~ 300 kHz.

In the literature, FE investigations are mostly carried out in a parallel plate setup, with diode or triode configuration, where current is averaged on a large sample area. Our setup, exploiting a very pointed anode, enables FE measurements over a limited circular region, whose radius is shorter than the tip-film distance d (see following). By taking into account the average CNT diameter and density, a maximum of 50 to 250 CNTs, for $d = 500$ nm, are expected to take part in the emission process.

In addition, the (sub)micrometric values of d , let a (macroscopic) field of a few hundreds $V/\mu m$ be attained with a low voltage source and electrons can be extracted by fields significantly higher than those of few tens $V/\mu m$ commonly used.

IV. FIELD EMISSION THEORY AND SIMULATION

A. Fowler-Nordheim theory

FE occurs when electrons from a solid tunnel through the surface potential barrier whose width is reduced by the application of an external electric field. The emission current depends on the electric field at the emitter surface (referred as microscopic or local electric field), E_S , and on the workfunction, Φ , i.e. the effective surface-vacuum barrier height. The Fowler-Nordheim model [31], derived for a flat metallic surface at 0 °K and assuming a triangular potential barrier, predicts an exponential behaviour of the emitted current:

$$I = S \cdot a \frac{E_S^2}{\Phi} \exp \left(-b \frac{\Phi^{3/2}}{E_S} \right) \quad (1)$$

where S is the emitting surface area, E_S is the uniform electric field on that surface and a and b are constants. When S is expressed in cm^2 , Φ and E_S respectively in eV and V/cm^2 , $a = 1.54 \cdot 10^{-6} \text{ AV}^{-2} \text{ eV}$ and $b = 6.83 \cdot 10^7 \text{ eV}^{-3/2} \text{ V cm}^{-1}$.

In a parallel plate configuration, the field E_S can be obtained from the applied potential V and the inter-electrode distance d as $E = V/d$. If the cathode is con-

stituted by an array of sharp tips, a field enhancement factor, γ , which takes into account the amplification occurring around their apexes, has to be introduced and

$$E_S = \gamma \frac{V}{d} \quad (2)$$

According to (1) and (2), a Fowler-Nordheim plot of $\ln(I/V^2)$ as a function of $1/V$ is a straight line, whose slope, $m = b\Phi^{3/2}d/\gamma$, and interception, $y_0 = \ln[aS\gamma^2/(\Phi d^2)]$, can, in principle, be used to estimate γ and Φ [32].

Although corrections [33, 34] are required to describe effects of non zero temperature, series resistance, extremely curved surfaces and non-uniform field enhancement factors or workfunctions, the basic FN theory has proven to be a good model to achieve a first-approximation understanding of the emission phenomena. For temperatures up to several hundred degree Celsius and fields in a large window, F-N model provides a good fitting to the I-V characteristics of several kind of emitters, included individual or in-film carbon nanotubes.

Due to our setup geometry, E_S is non-uniform, depending on the distance r from the point just below the tip apex (point P in Fig. 4). We will show that we can overcome this complication by introducing an effective emitting area S and tip correction factor k , whose values will be determined by means of a numerical simulation.

B. Electric field and FE behaviour

The electric field generated by an ideal conical tip, of the dimensions of our AFM probe at a bias voltage V , on a grounded flat graphite surface at distance d , was numerically calculated by MAXWELL [35], a software which solves electromagnetic problems by finite element analysis. Graphite was chosen for its conductivity comparable to that of a CNT film.

The result obtained for $d = 500$ nm and $V = 150$ V is shown in Fig. 5, where we can observe the electric field lines (top) and magnitude levels (bottom). As expected, the field is perpendicular to the graphite surface and its modulus $E_S(r)$ is a decreasing function of the distance r . $E_S(r)$ is plotted in Fig. 6 together with a tip correction factor $k(r)$ defined as $E_S(r) = \frac{V}{d} \frac{1}{k(r)}$. Notice that the electric field on the surface of the apex of a tip, with curvature radius ρ , is often expressed as $E_{Tip} = \beta V$, where $\beta = [k(0)\rho]^{-1}$ is called the field enhancement factor of the tip. The correction factor k , that we have introduced, depends on the geometry of the tip and is independent of the bias voltage V .

A numerical calculation based on the image charge method (see reference [36, 37]) for a hyperbolic tip similar to ours gives a value close to our $k(0) = 1.48$. By using $E_S(r)$ in combination with the FN formula (1), and, thanks to the radial symmetry, by dividing the emitting

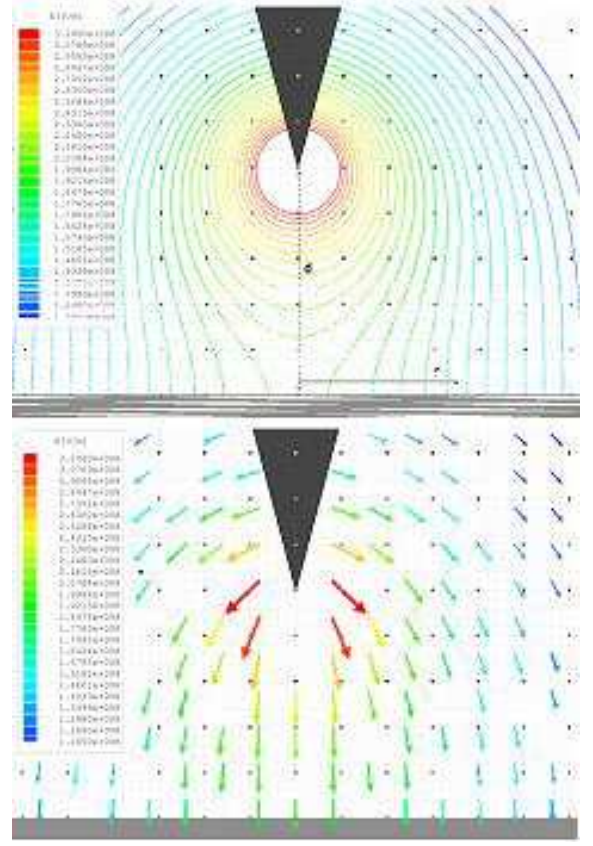


FIG. 5: Electric field (vector and magnitude distribution) generated by a metallic conical tip (30° aperture, 25 μ m height) on a flat graphite film. Tip-film potential difference 150 V, distance $d = 500$ nm.

surface in concentric annuli with center P, we obtained the predicted behaviour of the FE current. In the numerical calculation, we assumed $\Phi = 4.8$ eV as workfunction of the CNTs [38], while a constant field enhancement $\gamma_{eff} = 30$ was used to reproduce our experimental data since with a voltage bias of 150 V and at $d = 500$ nm we measured a current of about 10^{-5} A.

Fig. 7a shows that more than 99 % of the current is emitted from a circle of radius $r \leq d$, on which the field $E_S(r)$ is reduced by $\sim 38\%$ (while k varies from 1.48 to 2.0 (Fig. 7c)). The exponential behaviour implies that a modest variation of the field has a drastic effect on the value of the emission current.

Fig. 7b shows that maximum emission occurs from annuli of radius $r \sim d/3$ (thickness $dr = 0.5$ nm): field emission is initially dominated by the area increase, that, for $r \geq d/3$, is overwhelmed by the fall of the current density with increasing r .

Relative emission (i.e. percentage of the total) from a certain zone strongly depends on the applied voltage. To quantify this dependence, we report in Fig. 8 the fraction of the current, as a function of the bias voltage, that occurs from three circles, centered on P, of radius $d/2$, $2d/3$ and d , respectively. We can conclude that a

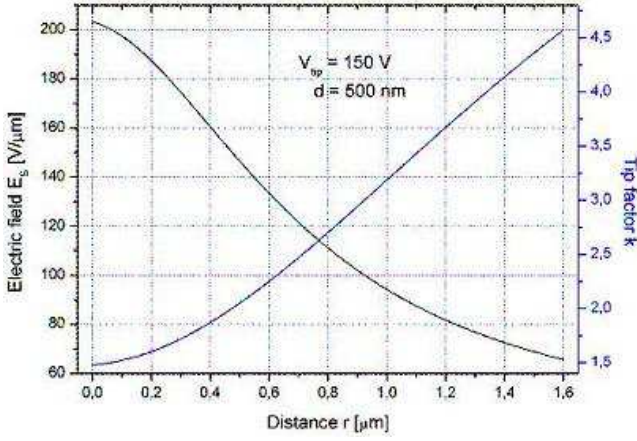


FIG. 6: Electric field magnitude $E_S(r)$ on the graphite film surface and tip correction factor $k(r)$ as a function of the horizontal distance r . Voltage bias 150 V, tip-flat surface distance 500 nm.

circle of radius $r \sim d$ is a very good estimation of emitting area over our entire sweeping voltage, while $r = 2d/3$ can be a sufficient value for applied voltages less than 100 V.

The calculated FE current versus the bias voltage and its corresponding FN plot are shown in Fig. 9. Remarkably, the FN plot is well fitted by a straight line, an expected result since

$$I = \int_0^\infty dr 2\pi r j(r) \approx \int_0^{r_{eff}} dr 2\pi r \frac{a\gamma^2}{[dk(r)]^2\Phi} V^2 \exp\left[-\frac{bd\Phi^{3/2}k(r)}{\gamma} \frac{1}{V}\right] \quad (3)$$

(with $r_{eff} \leq d$) makes I/V^2 an exponential function of $1/V$.

For $0 \leq r \leq r_{eff}$, we can neglect the variation of $k(r)$ and give it a constant effective value k_{eff} . Hence

$$I \approx \pi r_{eff}^2 \frac{a\gamma_{eff}^2}{[dk_{eff}]^2\Phi} V^2 \exp\left[-\frac{b\Phi^{3/2}d \cdot k_{eff}}{\gamma_{eff}} \frac{1}{V}\right] \quad (4)$$

By using our simulated data, we evaluate r_{eff} and k_{eff} from the slope m and the interception y_0 of the FN plot, which result respectively:

$$k_{eff} = \frac{m\gamma}{b\Phi^{3/2}d} \approx 1.6 \text{ and } r_{eff} = \frac{m e^{y_0/2}}{\sqrt{\pi a b \Phi}} \approx 300 \text{ nm.}$$

As a conclusion, we can analyze our experimental data using formula (4) with $k_{eff} \approx 1.6$ and $r_{eff} \approx \frac{2}{3}d$.

V. EXPERIMENTAL RESULTS AND DISCUSSION

A. I-V curves and FN plots

An example of a current-voltage characteristic measured by our apparatus is shown in Figures 10a-c. These

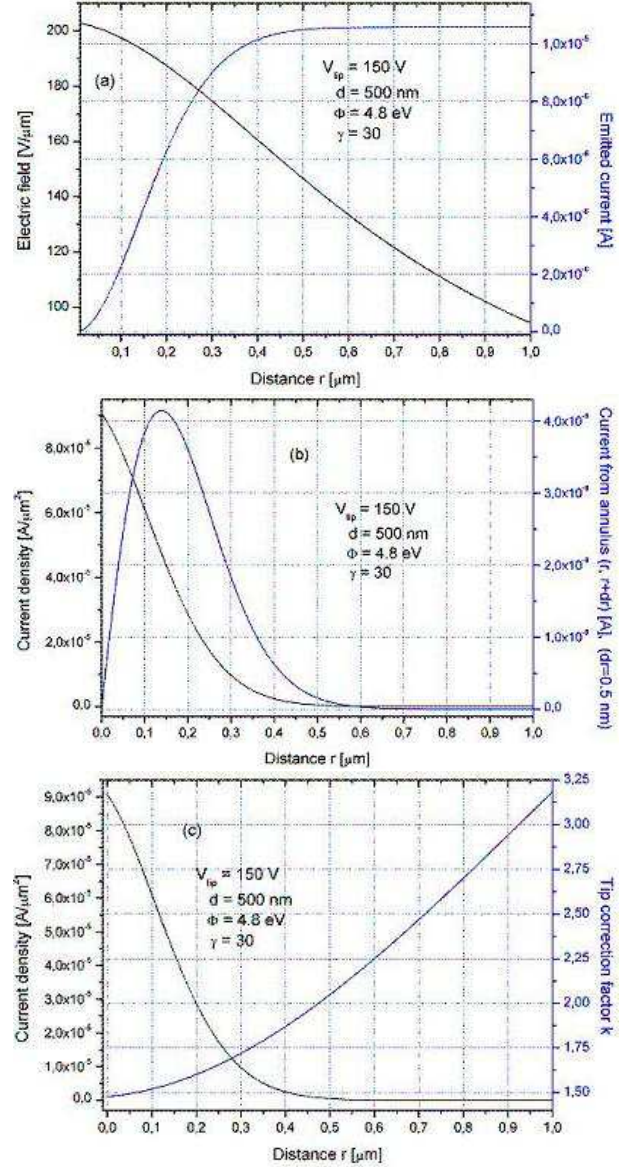


FIG. 7: Predicted FE current I , density of current J and current dI from annulus $(r, r+dr)$ as a function of the horizontal distance r . $dr=0.5$ nm in the numerical calculations.

data were obtained at a pressure of $\sim 10^{-4}$ mbar in non-contact mode by using an Au-coated AFM tip at a distance $d \approx 800$ nm from the CNT film surface and for an applied voltage stepping in the range $(-210, +210)$ V.

Above the sensitivity limit of our SMU (~ 1 nA at 100 V), we can observe a rapid rise of the current with the absolute value of the applied voltage. Indeed, electrons are extracted from the CNT film at voltages $\geq +120$ V, while for negative biases below -140 V, the current is field emitted from the AFM tip ;

The FE current from the CNTs occurs at a lower macroscopic electric field, is significantly larger and presents less fluctuations than that from the AFM tip, confirming the CNT film as a higher quality emitter. A

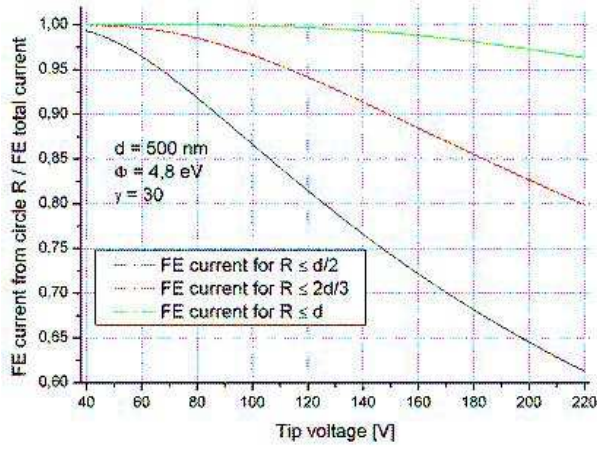


FIG. 8: Percentage of the FE current from circles of radius $R=d/2$, $2d/3$ and d and centered on P as a function of the bias voltage.

maximum current of $4.5 \cdot 10^{-5}$ A, corresponding to a current density $2-6 \cdot 10^3$ A/cm², is achieved without emitter failures. For the two sets of data (FE from CNT and tip), the different slopes ($m = \frac{k_{eff} b \Phi^{3/2} d}{\gamma}$) of the straight lines in the FN plot (Fig. 10c) can be attributed to a higher CNT field enhancement factor (gold has a workfunction of 5.28 eV, higher than that supposed for a MWCNT).

The distance d is measured from the approach point on the CNT film surface in AFM non-contact mode. The small force (1-10nN) applied by the tip to the surface in this modality likely does not change the local CNT topography by inducing displacements or vibrations of the highly moving and the flexible nanotubes. As already mentioned, the CNT topography and therefore the distance d can be affected by the application of the external voltage, which attracts the CNTs towards the tip. Consequently, the approach point is sometimes non reproducible and an accurate measurement of d is impossible. Furthermore Joule heating at high currents can modify the CNTs (sublimation of the walls, split off, severing, etc.) and again the distance d can vary. In what follows, we will consider the parameter d as merely indicative, and when possible, we will avoid using it in our quantitative analysis.

Assuming $\Phi = 4.8$ eV, from Fig. 10 c, we calculate $\gamma \approx 24$ and the microscopic field at which observable emission begins, $E_{turn-on}^{microscopic} \approx 2.2$ kV/ μ m.

A similar measurement, on the same sample, at high vacuum, $\sim 10^{-8}$ mbar, and with $d \approx 2$ μ m is shown in Fig. 11. After an electrical stress, consisting in a few voltage sweeps, necessary to stabilize the emission (see following), a series of 5 sweeps from 0 to 210 V was performed. Some negligible sweep-to-sweep variations were found, while, with respect to the measurements at lower vacuum, reduced single sweep fluctuations were observed.

The FN plot of Fig. 11 c1, for clarity showing only sweep 2, reveals an interesting deviation from linearity.

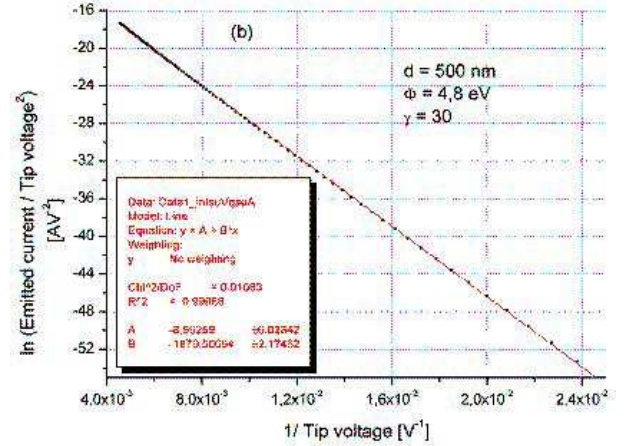
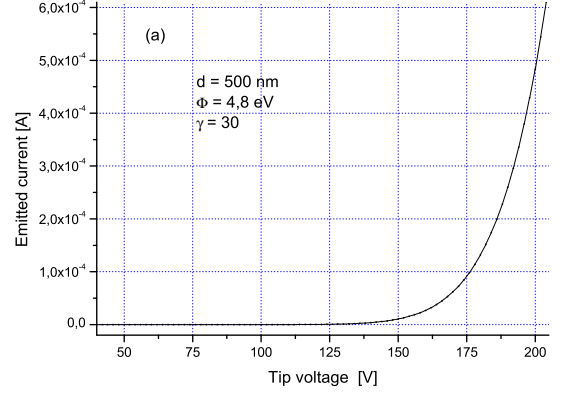


FIG. 9: Predicted FE current vs bias voltage and relative FN plot.

A change of slope (knee) appears at a bias of ~ 145 V (Fig. 11c) and corresponds to a sort of current saturation above 1 μ A (a closer look at Fig. 10 c shows a similar, but less pronounced knee, partially masked by the higher fluctuation level).

Saturation has been observed on individual multi-walled and single-walled nanotubes and to a lesser extend on nanotube films, and different explanations have been proposed [27, 28]. We ascribe this to a reduction of the applied field caused by the voltage drop on the series resistance R of the circuit model in Fig. 3.

Assuming R constant, formula (4) is modified as

$$I = c_1(V - RI)^2 \exp\left(-\frac{c_2}{V - RI}\right) \quad (5)$$

The constants c_1 and c_2 , which include γ_{eff} , r_{eff} and Φ , can be evaluated by fitting eq. (5) to the low emission current part of the experimental data, with $R = 0$. The result is shown in Fig. 11 c. In the chosen voltage range, 105-145 V, there is a very good agreement with the basic FN model.

Including the effect of the series resistance is not trivial. Equation (5) is recursive and has to be evaluated

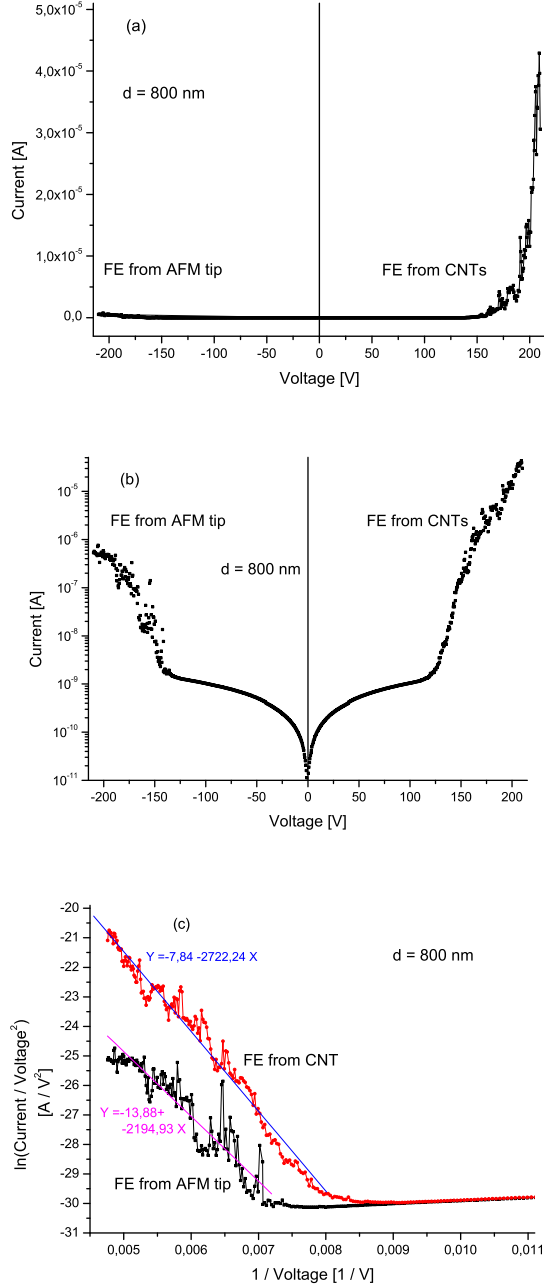


FIG. 10: Field emission current versus bias voltage in (a) linear and (b) logarithmic scale. (c) Fowler-Nordheim plot. Tip-CNT distance $d \approx 800$ nm, pressure 10^{-4} mbar, room temperature.

numerically, with R as fitting parameter. By numerical calculations, we were able to estimate a $R \approx 3.25 M\Omega$ and obtain the I-V characteristic shown in Fig. 11 c. With such R , Eq.(5) constitutes a good fitting to our data up to a voltage of about 190V; a rapid rise of the current is observed afterwards, likely due to additional nanotubes that enter the FN regime at such high electric fields.

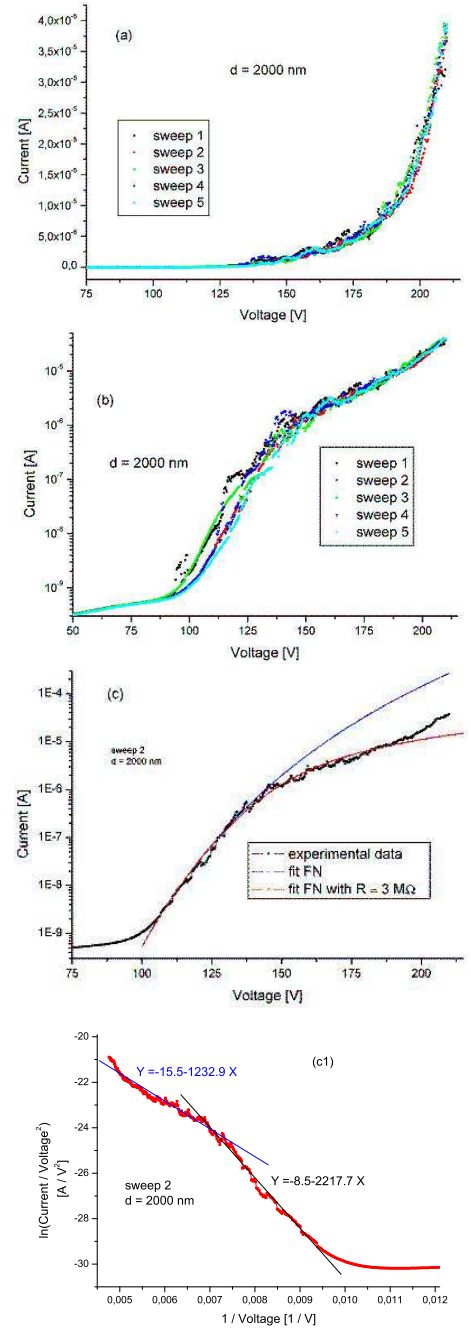


FIG. 11: Field emission current versus bias voltage in (a) linear and (b) logarithmic scale. (c) Current with FN and resistance modified FN fitting and (c1) Fowler-Nordheim plot for sweep 2. Tip-CNT distance $d \approx 2$ m, pressure $\sim 10^{-8}$ mbar, room temperature.

Possible origins for the resistor limited emission regime can be either a high internal resistance of the CNT, due to defects or heating for example, and/or to a resistive path to the SMU (resistance tube-to-tube, tube-to-substrate, CNT-to-metal and substrate-to-metal contact, etc.).

From the value of the emission current and of the volt-

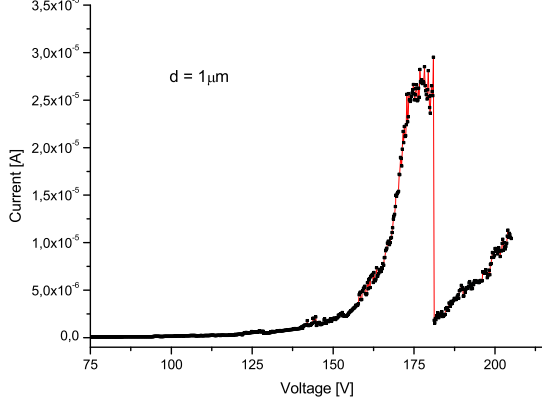


FIG. 12: I-V characteristic showing an event of high current degradation occurring at $V \approx 180$ V and $I \approx 30 \mu\text{A}$. Probably the emission after the degradation do not originate from the same tubes as before but from tubes nearby, which were before concealed by the original emitters.

age drop one can estimate the power dissipated on R, which is up to few mW in our measurements. This power is dissipated on a very small volume and can be sufficient to cause contact melting, detachment from the substrate, CNT severing, etc., with consequent emission degradation. An example of an event of high current degradation occurring at $I \approx 30 \mu\text{A}$ is shown in figure 12.

Finally, taking into account all the 5 sweeps, from the lower current part of the FN plot, a field enhancement factor $\gamma \approx 60 - 70$ and a $E_{\text{turn-on}}^{\text{microscopic}} \approx 2.0-2.2 \text{ kV}/\mu\text{m}$ can be evaluated.

The series resistance R can be expected to change across the film. Fig. 13 shows the I-V characteristics, with the applied voltage limited to 0-100 V to avoid degradation, where the effect of R, evaluated around 80 M Ω , is very pronounced. Actually we face a different phenomenon. At a current of $\sim 0.1 \mu\text{A}$, corresponding to a voltage of 50 V, a change of conduction mechanism occurs in the I-V characteristic: FE regime is followed by a pure ohmic increase of the current. A series resistance corrected FN model barely reproduces the I-V curve (Fig. 13 c). By referring to our model circuit, above $0.1 \mu\text{A}$, the field emission device seems to be replaced by a high value resistor. This seems to indicate that we were measuring in a region poor of CNTs or with CNTs damaged by previous electric stress and with lowered FE capability. This hypothesis is supported by the observation, through SEM analysis, of small spots of completely removed or simply shortened CNTs after uncontrolled electric stress. Fig. 14 shows zone (dark spot) where CNTs were completely removed by the passage of uncontrolled current during several attempts of setting the right parameters for the measurement of field emission maps (see following).

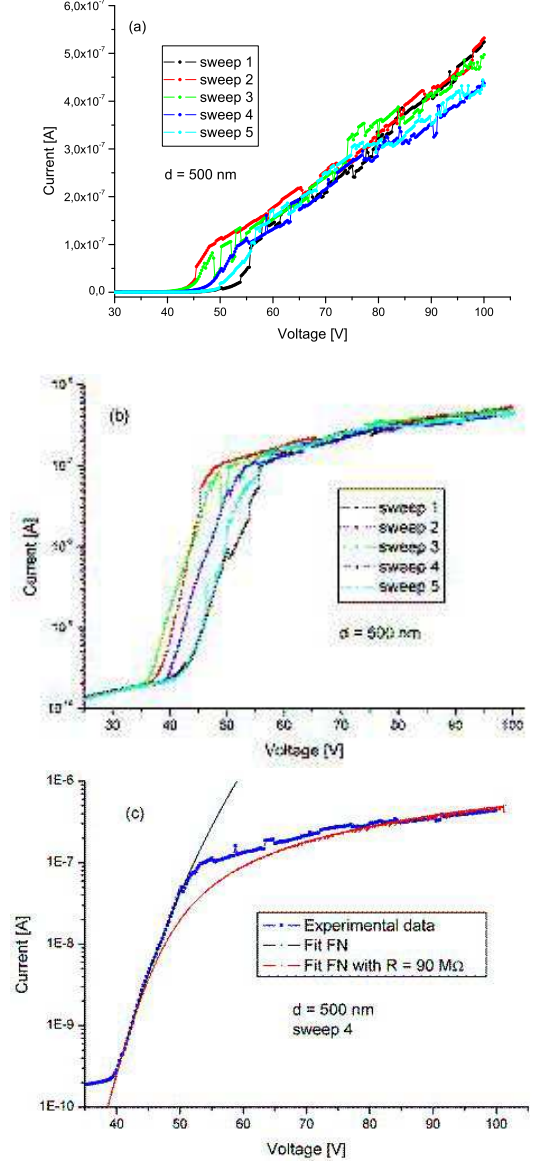


FIG. 13: Characteristics I-V with I in linear (a) and logarithmic scale (b,c). After a first steep rise (low current regime), a resistor limited emission regime (saturation) with $R \sim 80$ M Ω take place. Pressure 10^{-8} mbar, $d \approx 500$ nm. Room temperature.

B. Electrical stabilization

We systematically observed that the initial electrical sweeps on virgin zones have a positive conditioning effect: irreversible changes, in fact resulting in a stabilization, were found on the I-V characteristics.

An example is shown in Fig. 15. During the first sweep, a sudden rise of the current is observed around 30 V; after entering the μA range, the current suffers step-wise -up to one order of magnitude- drops and, at 210 V, its value is $\sim 17 \mu\text{A}$. Following sweeps show a completely

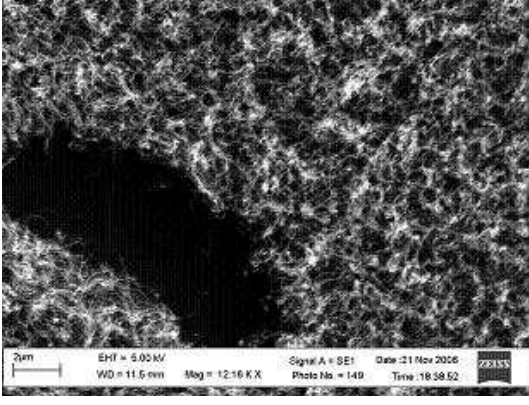


FIG. 14: Region of the film with CNTs pulled up or destroyed by electrical stress.

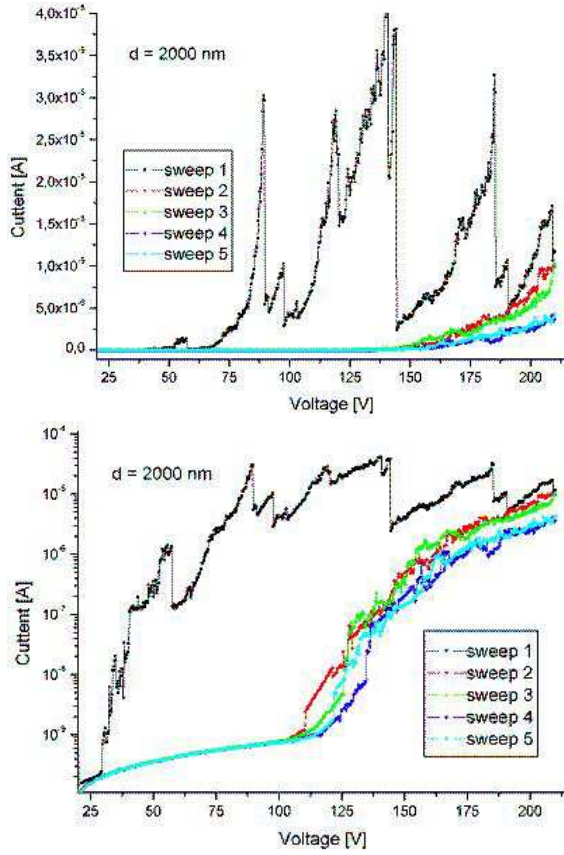


FIG. 15: Electrical conditioning showing the stabilization of the emission current by electric stress.

different behaviour, with higher turn-on voltage, 110-115 V, and considerably lower current (the higher the voltage the lower the current difference). For sweeps 2 and 3, at 210 V, a current of 10 μ A is measured; such current (\sim 4 μ A) is halved during sweeps 4 and 5.

We can attribute the higher current of sweep 1 to a single (or a few) longer nanotube(s) with dominant FE; a current around 1 μ A gradually degrades such tube(s),

till a complete destruction. After that FE becomes more stable.

Sometimes the stabilization process requires more sweeps.

A second example is shown in Fig. 16, where it is emphasized how the FN plot is evolving toward a straight line after an electrical conditioning. Apart fluctuations, the slope of the FN plot for sweep 1 and for the successive sweeps are comparable. This suggests that the field enhancement factor and the workfunction in both cases remain the same.

The slope of the FN plot, obtained from a fit of sweep 2, 3 and 4 together, can be used as usual to calculate the field enhancement factor, which results $\gamma \approx 23$.

In Fig. 16 b and c, the superposed (magenta) line refers to the prediction of the simulation based on a simple FN model (eq. 3), previously discussed. A little discrepancy of simulated and experimental data is observed at high current, since the effect of the series resistance was not included in the simulation.

In addition to destruction of thinner and longer nanotubes, other mechanisms involved in the electrical conditioning can be desorption of adsorbates caused by CNT heating, topography changes due to CNT stretching and re-orientation, particulate cleaning, etc.

Adsorbates [39, 40], as different types of gases, are always present at the CNT surface, creating nanoprotusions i.e regions of reduced workfunction and increased enhancement factor, where field emission begins at low electric fields. The formation and the electric field-driven surface diffusion of those nanoprotusions can cause the observed instabilities of the FE current. At large currents, the local temperature becomes high enough to evaporate some of the adsorbates, provoking drops in the FE current.

C. Field enhancement factor

The field enhancement factor is the typical figure of merit given to qualify field emitters. As pointed out in reference [41], γ is strongly dependent on the measurement setup and a significant comparison of γ values is possible only when measurements are performed under the same experimental conditions.

In our previous measurements, we evaluated γ from the slope m of the straight line fitting the data in the FN plots, $\gamma = \frac{b \cdot \Phi^{3/2} \cdot d \cdot k_{eff}}{m}$ assuming $\Phi = 4.8$ eV and $k_{eff} = 1.6$.

The field enhancement factor is known to be an increasing function of the inter-electrode distance and, taking into account our short d (0.5-2 μ m), we consider to have obtained rather high values of γ , likely due to the conspicuous length of our nanotubes. Published values range from few hundreds to several thousands, but at inter-electrode distances orders of magnitude higher than ours [42, 43, 44, 45].

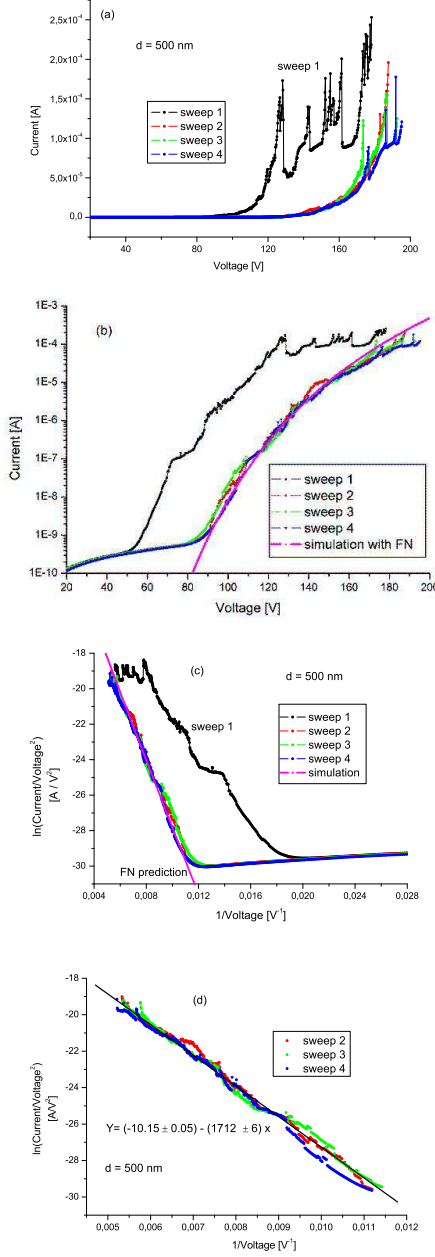


FIG. 16: FE for several voltage sweeps. Instabilities are reduced after first sweep and linearization of FN plot is obtained. (a) linear and (b) logarithmic current versus applied voltage, (c) Fowler-Nordheim plot (d) FN plot with linear fit for sweeps 2,3 and 4. Tip-CNT distance 500 nm. Room temperature.

Significant field screening effect (the applied electric field on the apex of a CNT is screened from the neighbouring CNTs [46, 47]) can be expected on our sample because of the high density of CNTs (it has been demonstrated that the optimal condition for high emission is a tube spacing twice the CNT length).

To investigate the dependence of the field enhancement

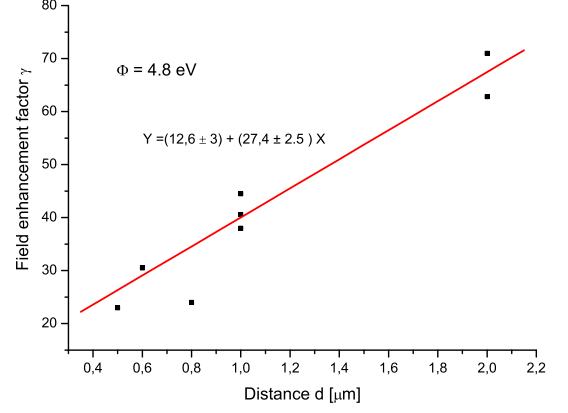


FIG. 17: Field enhancement factor as a function of the inter-electrode distance d .

factor on the inter-electrode distance, we estimated γ for several values of d . Despite the incertitude on the distance, we found a monotonic increase of γ with d ($\gamma \sim 60 - 70$ at $2\mu\text{m}$), as shown in Fig. 17. Linear extrapolation to larger values of d results in higher γ values than those found in Refs. [48, 49, 50].

D. MWCNT workfunction

The interception of the FN straight line with the y-axis can be used to evaluate the workfunction Φ as well:

$$\Phi = \frac{me^{y_0/2}}{\sqrt{\pi ab}} \cdot \frac{1}{r_{eff}} \quad (6)$$

Formula (6) assumes an accurate knowledge of the emitting area and of the interception y_0 (the exponential factor makes Φ very sensitive on y_0). Both those parameters are usually subjected to great incertitude and (6) provides a very rough estimation of Φ . Inversely, given Φ , one can use y_0 to evaluate the effective emitting area [51].

With that in mind, we took the data of Fig. 16 d, and by assuming $r_{eff} = 290$ nm as in our simulation, we calculated $\Phi \approx 3.5$ eV or, with $\Phi = 5$ eV, $r_{eff} \approx 200$ nm. Similar calculations made on other data samples produced results ranging from 2 to 10 eV.

It should be noticed also that Φ can vary across the film and can be affected by the presence of surface adsorbates or defects.

E. Turn-on field

To meaningfully compare field emitters, one usually reports the turn-on and the threshold fields, which are

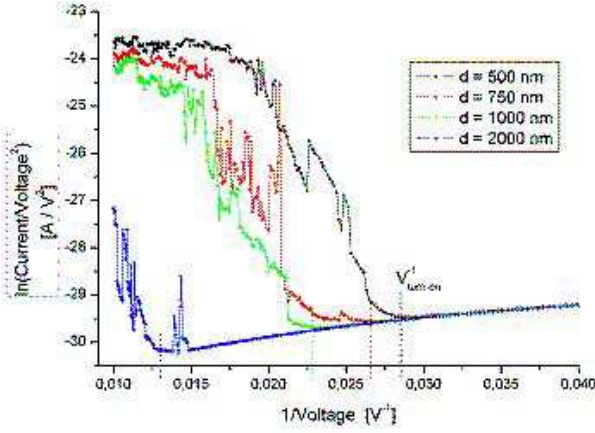


FIG. 18: Evaluation of the turn-on potential from FN plots with different nominal tip-CNT distances. The turn-on potential correspond to the point of upward bending. $P = 10^{-3}$ mbar, room temperature.

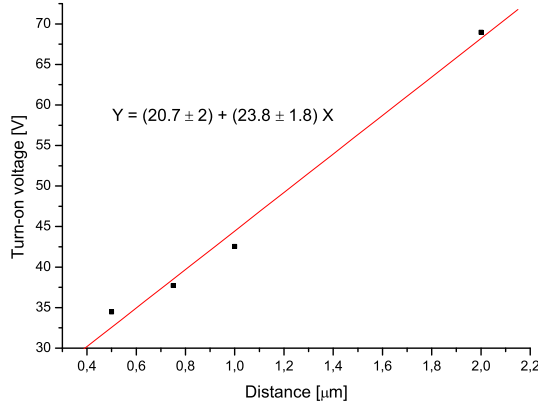


FIG. 19: Turn-on voltage as function of tip-CNT distance.

respectively defined as the macroscopic fields needed to extract current densities respectively of $10 \mu\text{A}\cdot\text{cm}^{-2}$ and $10 \text{mA}\cdot\text{cm}^{-2}$ (which are the current densities required to light or saturate a pixel in a display).

The lack of a precise evaluation of the current density forced us to adopt a different definition of the turn-on field: following reference [52], we defined the turn-on voltage as the one corresponding to the upward bending of the curve in the FN plot, i.e to the establishment of the FN emission regime, and then we estimated the macroscopic turn-on field from it.

Referring to Fig. 18, we estimated $V_{turn-on}^{-1}$ and then we calculated $E_{turn-on} = V_{turn-on}/(k_{eff}d)$. During the measurements, we started at $d = 1 \mu\text{m}$ and then we drove the sample by fixed steps to given distances. To rely only on those movements, we evaluated the turn-on field with a differential method, as $E_{turn-on} = \frac{1}{k_{eff}} \frac{\partial V_{turn-on}}{\partial d}$ ($E_{turn-on}$ is assumed constant on the range of d). Since,

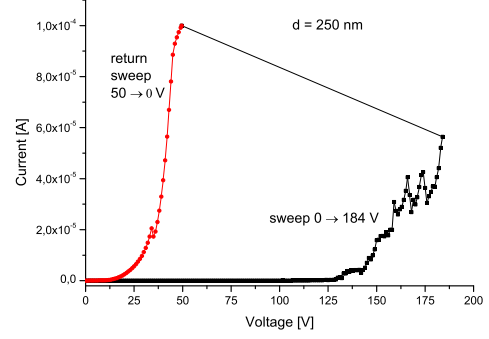


FIG. 20: I-V characteristic with the attachment of one or more nanotubes to the AFM tip, occurring at 184 V and producing a short circuit between the tip and the CNT film. The red curve is the one measured with AFM probe in contact with the CNT film. SMU current compliance 10^{-4} A.

the distance d is an unreliable parameter, we avoided it in our quantitative analysis by relaying on the steps of the piezoelectric displacing the sample.

A plot of $V_{turn-on}$ as a function of d (Fig. 19) can help evaluate the derivative, that equals the slope of the fitting straight line. This algorithm provides $E_{turn-on} \approx 15 \text{V}/\mu\text{m}$, a good figure considering the screening effect, which agrees with values obtained on similar MWCNT films (see for example Ref. [53]).

F. CNT capture

The bias voltage induces a considerable mechanical stress on an emitter of nanometric section. Even an applied field of few $\text{V}/\mu\text{m}$ has been proven to be sufficient to deflect and straighten carbon nanotubes [27].

The force applied during a sweep can be sufficient to reorient or even to peel nanotubes off. Sometimes a metal layer, Ta for example, is deposited under the catalyst to assure a better mechanical and electrical anchorage of the nanotubes to the substrate, a trick that we did not use.

The long nanotubes, attracted to the AFM tip, still attached to the substrate or pulled up but still in electric contact with film (because partially immersed in it), can create a conducting path between the probe and the film. Such phenomenon has been systematically observed for $d \leq 350 \text{ nm}$ while approaching higher voltages. An example is shown in Fig. 20: at 184 V, when a FE current of $57 \mu\text{A}$ is flowing, one or more CNTs are peeled off and attached to the AFM tip, causing a low resistive path between the probe and the film underneath, provoking a current jump to its compliance value (10^{-4}A). During the return sweep, below 50 V, the current follows the typical path it has with the probe in electric contact with the CNT film surface.

The tensile force applied on an infinitesimal area dA

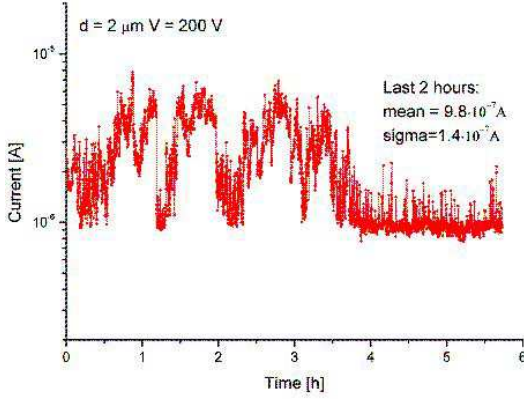


FIG. 21: Field emission current vs time. Applied Voltage 200V, tip-cnt distance $2\mu\text{m}$. $P = 10^{-7}$ mbar, room temperature.

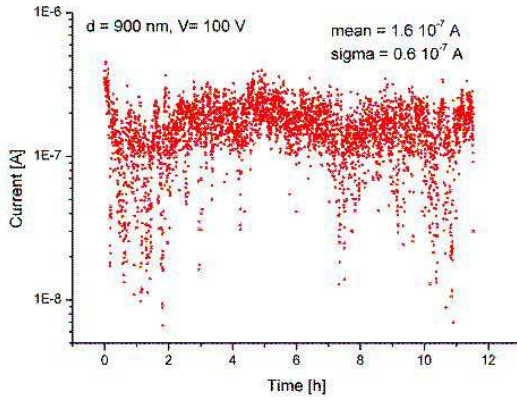


FIG. 22: Field emission current vs time. Applied Voltage 100V, tip-CNT distance 900 nm. $P = 10^{-7}$ mbar, room temperature.

by the electric field E_S can be expressed as $dT = (\epsilon_0/2)E_S^2 dA$. With the parameters of the experiment in Fig. 20, $E_S \approx \gamma \frac{V}{d \cdot k} \approx 1.4 \cdot 10^4 \frac{\text{V}}{\mu\text{m}}$, a stress of $\sim 8.7 \cdot 10^{-4} \text{N}/\mu\text{m}^2$ is applied. Hence, in correspondence of the emitter failure voltage, the tensile force on a typical nanotube of 30 nm diameter is $\sim 2.5\mu\text{N}$.

G. Time stability

The study of the emission current over time is very important for the utilization of CNTs in technological applications [54].

We measured the stability of field emission over periods of several hours, both in the high and low current regime.

Individual nanotubes are known to have high instabilities compared to dense films where current is averaged on an extremely large number of emitters [55]. In our setup, current is contributed by a limited number of emitters and for lack of "ensemble effect" enhanced fluctuations are expected.

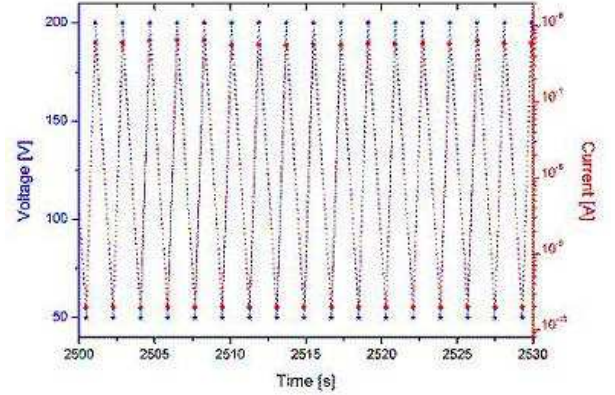
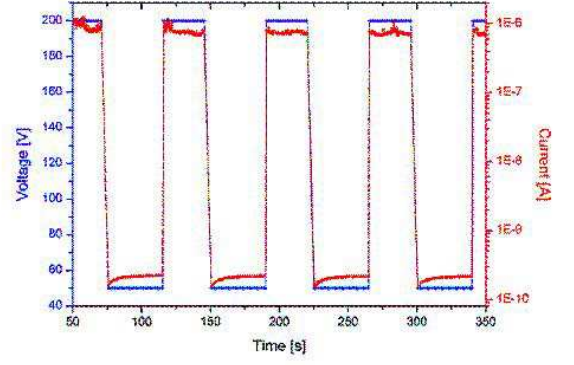


FIG. 23: Field emission current upon application of a pulsed and switching voltage. $P = 10^{-7}$ mbar, room temperature.

Fig. 21 shows the result obtained for emitters in the high current (or saturation) regime. A measurement was taken every 5 seconds. During the first 4 hours the current was fluctuating over an order of magnitude, with high frequency variations superposed to a sort of low frequency oscillation; a good stability of 15 % (one sigma), at the lowest current, was achieved afterwards.

It should be pointed out that operating the nanotubes in the current saturation regime is always risky as the current saturation is a sign of power dissipation and therefore of possible degradation, that might have been occurred during our measurement before stabilization.

In low current (non-saturation) regime, no overall decay in the emission current was observed over a period of 12 hours, as shown in Fig. 22 (where the current was measured every 20 s for 12 consecutive hours). A one sigma stability less than 30 % was achieved. This can be considered a good result compared to reported instabilities up to 50 % in the same regime [56, 57].

To investigate stability of field emission upon a changing voltage we measured the current with a low frequency pulsed and switching voltage for a few hours, obtaining results as those shown in Fig. 23. The FE current was found to follow the variations of the applied voltage over a time of about 3 hours without any failure.

H. Field emission under laser irradiation

The effects of laser irradiation on FE from MWCNTs is very interesting for the study of their optoelectronic properties and for their possible utilization in radiation detectors [58, 59]. Reference [60], for example, reports a marked increase of emission current with the irradiation duration (more than a factor 15 after 6 min irradiation with continuous wave (CW) 633 nm laser focused to a 5 mm spot size and with fluence of 10 mW) and suggests a laser induction of surface plasmons as possible explanation. To investigate laser effects, we compared FE

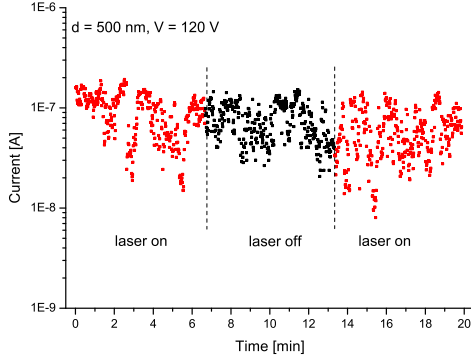


FIG. 24: FE current measured at given distance and voltage with and without laser irradiation of the emitting surface.

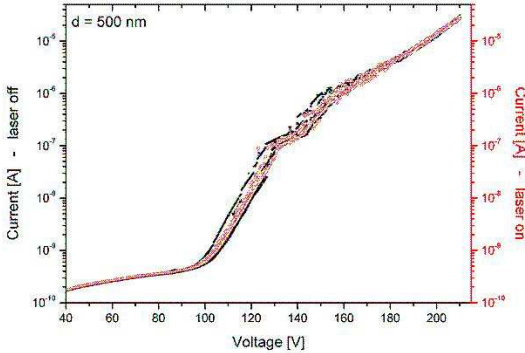


FIG. 25: I-V characteristic with and without laser irradiation of the emitting surface. Several voltage sweeps showed no significant FE current difference.

current with and without irradiation on several positions, after electric conditioning. CW lasers with wavelengths of 655 nm and 670 nm, 5 mW power and spot size of about 5 mm were used (the fluence was well below the threshold for destructing the CNTs). Comparison of signals with and without lightening (laser beam was almost parallel to the sample surface) did not show any significant difference, neither as a function of the irradiation duration neither as a function of the bias voltage (Fig. 24 and 25). However, we consider this experiment non-conclusive and we plan to repeat it with more powerful and different wavelengths lasers.

VI. SUMMARY

We have reported measurements of field emission from a vertical and quasi-aligned CNT film, produced by catalytic CVD, by using an original measurement setup based on a voltage biased AFM/STM nanometric probe. We were able to accurately characterize the local field emission behaviour, with currents averaged on a limited number of emitters. We have found that a modified Fowler -Nordheim model accounting for a series resistance provides a satisfactory explanation of the experimental results. We also gave an estimation of relevant parameters as field enhancement factor, MWCNT work-function and turn-on field. We studied FE stability and effects of red laser light.

Acknowledgments

We thank R. Fittipaldi and A. Vecchione for the SEM images and GINT (Gruppo INFN per le NanoTecnologie) collaboration for motivating and supporting this work.

- [1] E. L. Murphy et al., "Thermionic emission, Field emission, and the transition regime", *Phys. Rev.* 102 (1956) 1464-73
- [2] N.S. Xu et al., "Novel cold cathode materials and applications", *Mat. Sci. Eng., R* 48 (2005) 47-189
- [3] S. Yamamoto, "Fundamental physics of vacuum electron sources", *Rep. Prog. Phys.* 69 (2006) 181-232
- [4] V. N. Popov, "Carbon Nanotubes: Properties and application", *Mat. Sci. Eng., R* 43 (2004) 61-102
- [5] M. Meyyappan (ed), "Carbon Nanotubes: Science and applications", CRC Press, 2005
- [6] P.J.F. Harris, "Carbon Nanotubes and Related Structures", Cambridge University Press, 1999

- [7] B. Saito et al., "Physical Properties of Carbon Nanotubes", Imperial College Press.
- [8] M.P. Anantram et al, "Physics of carbon nanotube electronic devices", *Rep. Prog. Phys.* 69 (2006) 507-61
- [9] S. Iijima, "Helical microtubules of graphitic carbon", *Nature* 354 (1991) 56-58
- [10] J. M. Bonard et al., "Field emission from carbon nanotubes: first five years", *Solid-State Electronics* 45 (2001) 893-914;
- [11] J. M. Bonard et al., "Carbon nanotube films as electron field emitters", *Carbon* 40 (2002) 1715-1728

- [12] Y. Cheng, "Electron field emission from carbon nanotubes", *C. R. Physics* 4 (2003) 1021-1033
- [13] M.I. Shakir et al., "Carbon nanotube electric field emitters and applications", *Nanotechnology* 17 (2006) R41-R56
- [14] S. H. Jo et al., "Effect of length and spacing of vertically aligned carbon nanotubes on field emission properties", *Appl. Phys. Lett.* 82 (2003) 3520-22
- [15] S.C. Lim et al., "Field emission properties of vertically aligned carbon nanotube array dependent on gas exposure and growth conditions", *J. Vac. Sci. Technol. A* 19 (2001) 1786-1789
- [16] J.T.L. Thong et al., "High current field emission from a vertically aligned carbon nanotube field emitter array", *Appl. Phys. Lett.* 79 (2001) 2811-13
- [17] S. H. Jo et al., "Correlation of field emission and surface microstructure of vertically aligned carbon nanotubes", *Appl. Phys. Lett.* 84 (2004) 413-415
- [18] M. Sveningsson et al., "Electron field emission from multi walled carbon nanotubes", *Carbon* 42 (2004) 1165-68
- [19] Y.Y. Wang et al., "Growth and field emission properties of small diameter carbon nanotube films", *Diamond and Related Materials* 14 (2005) 714-718
- [20] P. Sarrazin, "Field emission" in *Carbon nanotubes: science and applications*, edited by M. Meyyappan, CRC Press 2005, pp 195-212
- [21] Y. Saito et al., "Field emission from carbon nanotubes and its applications to electron sources". *Carbon* 38 (2000) 169-182.
- [22] Y. Saito et al., "Field emission of carbon nanotubes and its application as electron sources of ultra-high luminance light-source devices", *Physica B* 323 (2002) 30-37
- [23] G. N. Fursey, "Field Emission in vacuum electronics", *Appl. Surf. Sci.*, 215 (2003) 113-134
- [24] J.L. Kwo et al., "Characteristics of flat panel display using carbon nanotubes as electron emitters", *Diamond and Related Materials*, 9 (2000) 1270-74
- [25] L. Nilson et al., "Scanning field emission from patterned carbon nanotubes films", *Appl. Phys. Lett.* 76 (2000) 2071-73
- [26] L. Nilson et al., "Microscopic characterization of electron field emission", *J. Vac. Sci. Technol. B* 20 (2002) 326-337
- [27] J. M. Bonard et al., "Degradation and failure of carbon nanotube field emitters", *Phys. Rev. B* 67 (2003) 115406-1-10
- [28] P. Groning et al., "Carbon Nanotubes for Cold Electron Sources", *Adv. Eng. Mat.*, 5-8 (2003) 541-50.
- [29] M. Meyyappan et al., "Carbon Nanotube growth by PECVD: a review", *Plasma Source Sci. Technology*, 12 (2003) 205-16
- [30] C. Kim et al., "The effect of gas adsorption on field emission mechanism of carbon nanotubes", *J. Am. Chem. Soc.* 124 (2002) 9906-11
- [31] K.L. Jensen, "Electron emission theory and its application: Fowler-Nordheim equation and beyond", *J. Vac. Sci. Tech. B* 21- 4 (2003) 1528-1544
- [32] L. M. Peng et al., "On the phenomenological nature of the work function as determined from electron field emission experiments on nanotubes and nonowires", *Surface and Interface Analysis*, 38 (2006) 1073-77
- [33] C. J. Edgcombe, "Development of Fowler Nordheim theory for a spherical field emitter", *Phys. Rev. B* 72 (2005) 045420-1-7
- [34] C. J. Edgcombe et al., "Current voltage characteristics of nonplanar cold field emitters", *J. Vac. Sci. Tech. B* 21 (2003) 1519-23
- [35] MAXWELL is a software by Ansoft Corporation (Pittsburg, Four Station Square, Suite 200, PA 15219) which solves two or three dimensional electromagnetic problems through finite element analysis
- [36] G. Mesa et al., "Image charge method for electrostatic calculations in field emission diodes", *J. Appl. Phys.* 79 (1996) 39-44
- [37] J.D.Zuber et al., "An analytical solution for microtip field emission current and effective emission area", *J. Appl. Phys.* 91 (2002) 9379-9384
- [38] R. Gao et al., "Work function at the tips of multi-walled carbon nanotubes", *Appl. Phys. Lett.*, 78-12 (2001) 1757-59
- [39] K.S. Yeong et al., "Effects of adsorbates on the field emission current from carbon nanotube", *Appl. Surf. Sci.*, 233 (2004) 20-23;
- [40] V. Semet et al., "Field electron emission from individual carbon nanotubes of a vertically aligned array", *Appl. Phys. Lett.* 81 (2002) 343-345;
- [41] J. M. Bonard et al., "Can we reliably estimate the emission field and field enhancement factor of nanotube film field emitters", *Diamond and Related Materials* 11 (2002) 763-768
- [42] Z. Xu et al., "Geometrical enhancement of field emission of individual nanotubes studied by in situ transmission electron microscopy", *Appl. Phys. Lett.*, 88 (2006) 133107
- [43] J. Y. Huang et al., "Giant field enhancement at carbon nanotube tips induced by multistage effect", *Appl. Phys. Lett.* 87 (2005) 053110-1/3
- [44] H. J. Jeong, "Fabrication of efficient field emitters with thin multiwalled carbon nanotubes using spray method", *Carbon* 44 (2006) 2689-2693
- [45] S.C.Lim et al., "Extracting independently the work function and field enhancement factor from thermal field emission of multi-walled carbon nanotube tips", *Carbon* 43 (2005) 2801/07
- [46] J. Such et al., "Study of the field-screening effect of highly ordered carbon nanotube arrays", *Appl. Phys. Lett.* 80 (2002) 2392
- [47] M. Wang et al., "Field enhancement factor for carbon nanotube array", *J. Appl. Phys.* 98 (2005) 014315-1/4
- [48] S.M.C. Vieira et al., "Investigation of field emission properties of carbon nanotube arrays defined using nanoimprint lithography", *Appl. Phys. Lett.* 89 (2006) 02211-1/3
- [49] H.S. Uh et al., "Growth and field emission properties of carbon nanotubes on rapid thermal annealed Ni catalyst using PECVD", *Diamond and Related Materials* 14 (2005) 850-854
- [50] J. T. L. Thong et al., "High current field emission from a vertically aligned carbon nanotube field emitter array", *Appl. Phys. Lett.* 79 (2001) 2811-13
- [51] R. G. Forbes, "Field emission: New theory for the derivation of emission area from a Fowler-Nordheim plot", *J. Vac. Sci. Techn. B* 17 (1999) 526-33
- [52] J. L. Kwo et al. "Characteristics of flat panel display using carbon nanotubes as electron emitters", *Diamond and Related Materials* 9 (2000) 1270-4
- [53] E. Kowalska et al., "Electron emissive properties of CNT films grown by catalytic method on different types of substrates", *Diamond and Related Materials* 13 (2004) 1008-11

- [54] B. Ulmen et al., "Stability of Field Emission Current from various type of carbon nanotube films", *Diamond and Related Materials* 15 (2006) 212-216
- [55] J. M. Bonard et al., "Field emission from carbon nanotubes: perspectives for applications and clues to the emission mechanism", *Appl. Phys. A* 69 (1999) 245-254
- [56] Y. Saito, "Field emission from carbon nanotubes and its application to electron source", *Carbon* 38 (2000) 169-82
- [57] P. G. Collins et al. "A simple and robust electron beam source from carbon nanotubes", *Appl. Phys. Lett.* 69 (1996) 1969-71
- [58] J.M. Xu, "Highly ordered carbon nanotube arrays and IR detection", *Infrared Physics and Technology* 42 (2001) 485-491
- [59] L. Liu et al., "Multiwall carbon nanotube as a new infrared detected material", *Sensors and Actuators A* 116 (2004) 394-397
- [60] H. F. Cheng et al. "Laser irradiation effect on electron field emission properties of carbon nanotubes", *Diamond and Related Materials*, 13 (2004) 1004-7